

# Early Stages of Drop Coalescence

Antoine Deblais,<sup>1,\*</sup> Kaili Xie,<sup>1</sup> Peter Lewin-Jones,<sup>2</sup> Dirk Aarts,<sup>3</sup>  
Miguel A. Herrada,<sup>4</sup> Jens Eggers,<sup>5</sup> James E. Sprittles,<sup>2</sup> and Daniel Bonn<sup>1</sup>

<sup>1</sup>*Van der Waals-Zeeman Institute, Institute of Physics, University of Amsterdam, 1098XH Amsterdam, The Netherlands.*

<sup>2</sup>*Mathematics Institute, University of Warwick, Coventry CV4 7AL, United Kingdom.*

<sup>3</sup>*Department of Chemistry, Physical and Theoretical Chemistry Laboratory,  
University of Oxford, South Parks Road, Oxford OX1 3QZ, United Kingdom.*

<sup>4</sup>*Escuela Técnica Superior de Ingeniería, Universidad de Sevilla, Seville 41092, Spain*

<sup>5</sup>*School of Mathematics, University of Bristol, University Walk, Bristol BS8 1 TW, United Kingdom.*

(Dated: February 2, 2024)

Despite the large body of research on coalescence, firm agreement between experiment, theory, and computation has not been established for the very earliest times following the initial contact of two liquid volumes. Combining a range of experimental and computational modelling approaches, we have been able to elucidate the influence of the intervening gas, of the van der Waals forces and of thermal fluctuations on coalescence. For simple liquids, the gas influences both pre- and post-contact regimes, with a jump-to-contact the primary mode of merging. Subsequently, wave-like air pockets are observed. For a system with ultralow interfacial tension, that mimics nanodrop behaviour, the very first moments are governed by thermal fluctuations at the interfaces, with a nontrivial opening speed given by stochastic thermally driven motion.

The merging of liquid volumes is important for a plethora of fluid phenomena: for example, drop-drop coalescence dynamics dictate the size of raindrops, efficacy of virus transmission, accuracy of inkjet printing and efficiency of spraying phenomena [1–5], whilst drop-surface interactions are key for production of ocean mist, air-sea gas exchange and airborne salt particles [6, 7].

When colliding drops are able to displace the surrounding gas to touch, coalescence is initiated with the formation of a liquid bridge (or neck) between the two drops, which subsequently grows, with surface tension driving the expansion. Depending on the parameter regime, namely whether it is the drop’s viscosity or inertia that resists capillary forces, different scaling have been derived for this growth [8, 9].

In the conventional hydrodynamic description of coalescence, the growth is initially inhibited by the viscosity  $\eta$  of the liquid. The rate of growth is then determined by a balance of capillary and viscous forces, and a simple dimensional analysis then leads directly to a capillary velocity  $U_{cap} \approx \gamma/\eta$ , with  $\gamma$  the surface tension, which gives the rate at which the fluid bridge increases. A more detailed analysis [8] shows that there is a logarithmic correction to this, leading to a temporal variation of the bridge radius  $R \propto \tau \log \tau$ , where  $\tau = t - t_0$  is time from initial contact.

For the coalescence of water droplets ( $\gamma \approx 70$  mN/m and  $\eta = 1$  mPa s),  $U_{cap} \approx 70$  m/s. This means that very rapidly the fluid inertia becomes important; the balance between inertial and viscous forces is dictated by the local Reynolds number  $Re(\tau) = \rho \gamma R^2 / R_0 \eta^2$  with  $\rho$  the density,  $R(\tau)$  the neck/bridge radius and  $R_0$  the drop radius [10]. For mm-sized drops of water,  $Re \approx 1$  when  $R \approx 1 \mu\text{m}$ . Thus, for water the viscous regime is hard to observe, and the coalescence is, from a practical point of view, mostly inertial. The inertial dynamics is then given by  $R(\tau) \approx A(\gamma R_0 / \rho)^{1/4} \tau^{1/2}$ , where the prefactor

$A$  derived from experiments can take different values [1.1–1.25] [9, 11, 12].

For drop-drop coalescence, for sake of argument, these classical theories assume that the initial state consists of two stationary undeformed spherical drops joining at a point. But how do these drops actually displace the intervening gas and come into contact?

Experimentally, this is a very difficult question as direct imaging is evidently limited by both the optical resolution and the rate at which images can be acquired [9, 13]. In addition, focusing on the plane of the coalescing drops and ‘seeing into’ its cusp-like region may lead to spurious exponents for the dynamics, as shown in [14]. To overcome these issues, Paulsen *et al.* [10, 15] deployed an electrical method to infer the bridge radius in the early stages and proposed a new initial regime in which inertia, capillarity and viscosity are all important. However, simulations of the full Navier-Stokes system [16, 17] show no evidence for this regime, so that links between experiment and theory remain unclear.

In this Letter, we study the initial stages of drop coalescence at extremely short ( $\approx 0.1 \mu\text{s}$ ) time and length ( $\approx 2 \mu\text{m}$ ) scales and in a system with ultralow surface tension ( $\approx 5$  nN/m); the latter to investigate the effect of thermal fluctuations. A new imaging arrangement allows us to show that the rupture of an air film, the merging of a drop with a bulk liquid happens with a jump into contact, and capillary waves are generated at the liquid surface ahead of an entrapped air pocket. The ultralow tension system shows two types of coalescence. For relatively high surface tension, the coalescence is viscous; however for the lowest surface tension, thermal-fluctuation-driven capillary waves are clearly visible, and these govern the very early stages of coalescence, leading to a novel fluctuation dominated coalescence regime with a nontrivial dependence of the neck radius on time.

**Drop-Drop.** We use an electrical technique similar to those described in [10, 15, 18, 19] to measure the coalescence between two drops. In order to increase the spatial and temporal resolution of this measurement, we use salt water with a large

\* A.Deblais@uva.nl

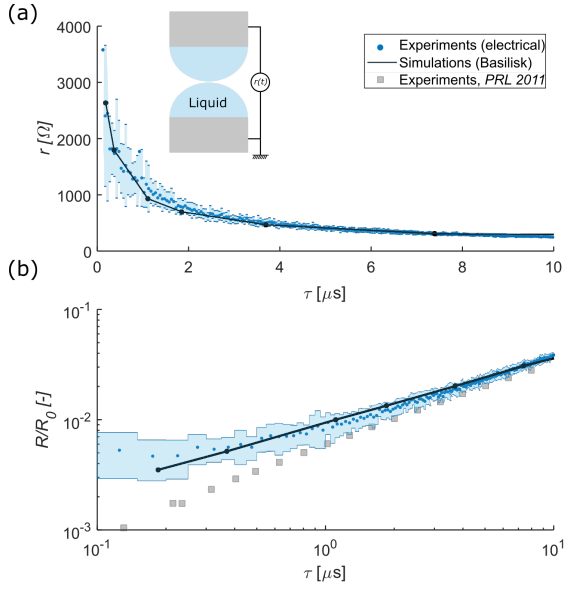


**FIG. 1. Temporal coalescence dynamics of liquid droplets probed with an electrical method.** (a) Electrical resistance  $r$  of a low-viscous saline capillary bridge ( $\eta = 1.8$  mPa s) between two electrodes ( $R_0 = 1$  mm) as a function of time. The upper electrode moves at very low constant downwards speed, initiating coalescence; the electrical resistance is obtained from the complex impedance of the circuit, following the method detailed in [15]. (b) From the electrical resistance shown in (a), the opening dynamics of the neck can be obtained (Eq. 1 of Ref. [15]). Data from Ref. [10] are plotted for a comparable low-viscous liquid ( $\eta=1.9$  mPa s). Dots represent averaged values, while the shaded area corresponds to standard deviations.

conductivity, allowing us to reach submicron spatial and almost nanosecond temporal resolution. In Fig. 1(a) we plot the measured conductivity as a function of time. The shape of the liquid bridge is computed from a simulation, allowing us to calculate the resistance  $r$  of the neck in time. We used a numerical scheme based on a volume-of-fluid (VOF) method provided by the ‘Basilisk’ software [20] which uses QUADTREES [21] to allow efficient adaptive grid refinement of the interface close to the coalescence region (see more details in Supplemental Material, Sec. I and Sup. Fig. S1). The measured resistance of the liquid bridge data is well described by the simulations at early stage of the coalescence point.

Fig. 1(b) shows the minimum neck radius  $R/R_0$  as a function of time after coalescence as follows from the electrical measurements: the neck diameter is obtained from the relation  $R = 2[(r - 1/\pi R_0 \sigma)3.62\sigma]^{-1}$  (Eq. 1 of Ref. [10]), which we also confirmed from our simulation (see Sup. Fig. S4 in the Supplementary Material). The dynamics follow the form  $R(\tau) \propto \tau^\alpha$ , and for which we recover  $\alpha = 0.5$  for the inertial case. For the inertial regime, it was previously found that  $R(\tau) \approx 1.1(\gamma R_0/\rho)^{1/4}\tau^{1/2}$ . We attribute the different slope observed in Ref. [10] to be due to the initial deformation of the interface due to the presence of charges (see Sup. Fig. S5). Our first data point for water in this regime is  $\approx 10$   $\mu\text{m}$  at  $\approx 1$   $\mu\text{s}$ , which is very close to what is expected from the equa-

tion. This is in agreement with findings from [10]; however, in the absence of optical imaging we have no information about how the initial contact occurs or the subsequent shape of the interface.

To access this initial pre-contact approach stage, we deploy bespoke finite element simulations which include the influence of the gas, with corrections due to kinetic effects for microscale gas films, alongside van der Waals effects, see [22] for details of the computational framework. In Sup. Fig. S2, we see that for the slow approach speeds considered in our experiments, the deformation of the drops caused by gas lubrication is relatively small so that the interfaces meet at  $r = 0$ , *i.e.* no bubble is entrapped. Notably, the van der Waals force causes a ‘jump to contact’ when the separation of the drops is  $\approx 30$  nm over a timescale of  $\sim \mu\text{s}$ . This ‘jump into contact’ for separations of  $\sim 10$ ’s of nm is consistent with the literature [23–26] and was previously observed for AFM tips connecting to a fluid surface.

**Drop-Bath.** To access the initial stages of coalescence optically, we turn to the drop-bath phenomenon and use a novel approach by viewing the event from ‘underneath’ (impossible for drop-drop) to overcome spurious effects due to side imaging [14, 27], where it is not possible to measure small contact radii (less than 20  $\mu\text{m}$  for instance) due to the unfavorable spherical geometry of the droplet and optical effects [9, 14, 26, 27]. The setup consists of a drop on a needle to which liquid is supplied slowly by a syringe pump. This drop is facing a bath of the same liquid (see Sup. Fig. S7). Our needle tip is millimetric (diameter 1.37 mm) and a drop is slowly grown at its tip until it coalesces with the bulk (growing velocity  $\leq 20$   $\mu\text{m/s}$ , in an attempt to minimize the effect of air drainage between the droplet and the bulk surface). To change the properties of the fluids, different amounts of glycerol were mixed with deionized water (Milli-Q). The viscosity, density and surface tension are given in the Supplementary Table S1. All experiments were performed at room temperature ( $22 \pm 1$   $^\circ\text{C}$ ) and atmospheric pressure.

The growth of the neck bridging the droplet with its bulk is recorded from below through the bath using an inverted microscope (Zeiss Axiovert A1) at a frame rate of up to 1,000,000 frames per second (fps) using a high-speed camera (Phantom TMX 7510) allowing us to reach a spatial resolution of typically 0.9  $\mu\text{m}/\text{pix}$  with a  $20\times$  microscope objective (Zeiss long working distance WD = 20mm). The minimum neck radius  $R$  is followed in time with a simple homemade routine (Fig. 2).

Fig. 2(a) shows a sequence of the neck opening during coalescence for the droplet-bulk geometry exhibiting two features. It is immediately clear that (i) there is an abrupt change of intensity which corresponds to the coalesced/bridge radius and (ii) there are also concentric rings ahead of the bridge, see Fig. 2(b), which appear to be the signature of interfacial waves that refract passing light. This is confirmed by examining the interface profile obtained from the Basilisk simulations at a specific time ( $\tau = 64$   $\mu\text{s}$ ), as shown in Fig. 2(c), where waves are observed ahead of an air pocket (see also Sup. Fig. S6). This combination of inertial coalescence driving wave formation and gas lubrication preventing the pinch-off of toroidal

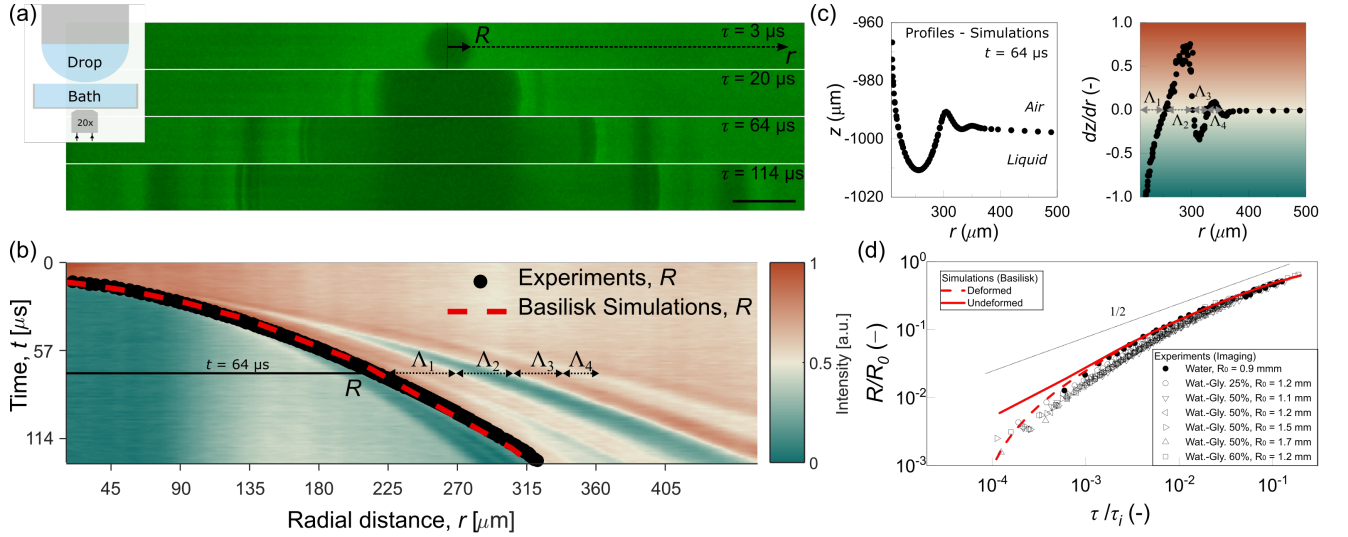


FIG. 2. **Temporal Coalescence Dynamics of Droplet-Bulk Probed Optically.** (a) Image sequences captured from the bottom view using the fast camera. The photographs depict the very early stages of bath interface coalescence, where the droplet (water,  $R_0 = 0.9$  mm) contacts the lower bath. The artificial green color is applied solely for improving image contrast. (b) Corresponding spatio-temporal averaged intensity of (a). Black dot points indicate the tracked minimum neck diameter  $R$ , and the dashed red line represents the Basilisk simulation for the same droplet radius  $R_0$  as in (a). As the minimum neck diameter increases, capillary waves are excited ahead of the front, as shown by the change in intensity. (c) Profiles of the interface extracted from the simulation at  $\tau = 64 \mu\text{s}$  after coalescence (left), and its corresponding first derivative (right). We define the lengths  $\Lambda_i$  for which the local derivative is either positive or negative. These lengths correspond to the change in intensity observed in (b) due to the refraction of light at the bath interface. (d) Rescaled radius (with the initial drop radius  $R_0 = [0.9; 1.73]$  mm) versus rescaled time (with the inertial time  $\tau_i = \sqrt{\rho R_0^3 / \gamma}$ ) for the different liquids investigated and for three different initial drop sizes (for the fluid with viscosity 5.7 mPa·s).

bubbles has been described previously [16, 28], and is also predicted for viscous coalescence [8], but strong direct experimental evidence for it has been lacking until now.

To further confirm this hypothesis, in Fig. 2(c) we plot the spatial deformation ( $dz/dr$ ) obtained from the simulations, in order to define domains  $\Lambda_i$  where the interface undergoes pronounced changes, and show in Fig. 2(b) we show that this aligns with experimental changes in intensity.

As shown in Fig. 2(d), different viscosities of fluids (range from 1 mPa·s to 11.5 mPa·s) were tested. In the late stage of coalescence, the inertial-capillary regime is found, the same as we observed in the electrical measurement  $R(\tau) \sim \tau^{1/2}$ . In the early stage, a different regime is observed for all fluids, with a radius that is smaller than would be expected from the inertial-capillary regime. For the earlier regime, all the curves collapse when scaled with the inertial time: there is no effect of viscosity, and the differences in [Fig. 2(d)] are due to differences in density and surface tension (See Sup. Table 1).

Basilisk simulations (red line) of the droplet-bulk coalescence for water, agree quantitatively well with our experimental measurement overall the whole range of times. However, to achieve this agreement, the time axis in the simulation has been set to match the experiments [Fig. 2(b)] and we also adjusted the minimum neck diameter  $R$  by  $50 \mu\text{m}$  to align the experiments with the simulations. Adjusting the time is rather standard, and amounts to fixing the coalescence time  $t_0$ , but the reasons for the spatial shift remains unclear and motivated us to look into the pre-contact dynamics...

In our experiments, we observe interference fringes between the two surfaces in the last frames before coalescence (see Sup. Fig. S8), which suggest the presence of a thin air film which acts as a lubricant between the two approaching surfaces. This air film continually thins, and if it becomes thin enough, the two surfaces jump into contact. This behaviour

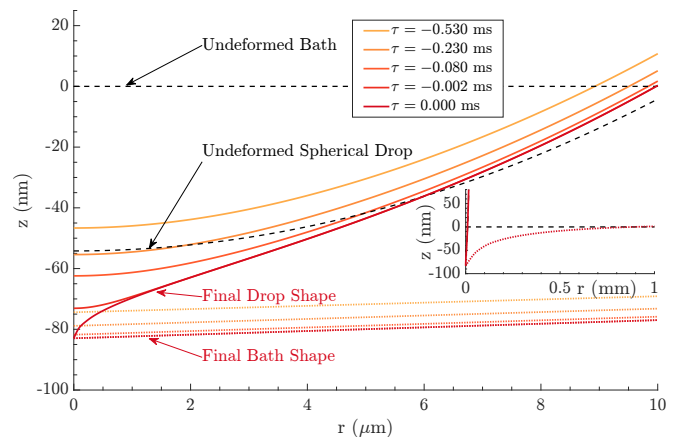


FIG. 3. Computed interface profiles of the final stages of a drop moving towards a liquid bath at  $5 \times 10^{-6}$  m/s, before coalescence with first contact occurring at  $\tau = 0$ . It shows the deformation of the bath and the 'jump to contact'. Model parameters are the same as those for the drop-drop case in Sup. Fig. S2.

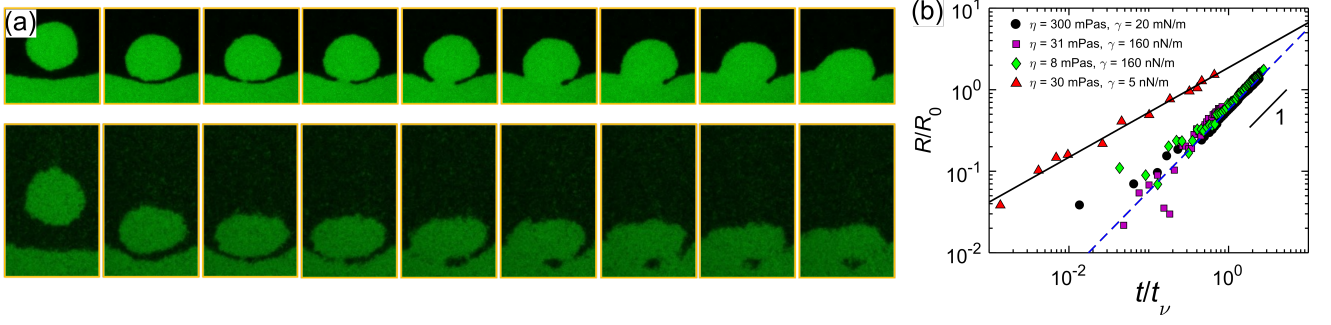


FIG. 4. **Temporal coalescence dynamics of colloidal liquid droplets.** (a) Sequence of pictures showing the dynamics of coalescence for  $\gamma \approx 160$  nN/m (upper panel) and for  $\gamma \approx 5$  nN/m (bottom panel). Top row, droplet of diameter 16.5  $\mu\text{m}$ ; bottom row, 21.8  $\mu\text{m}$ . Data are extracted from [29]. (b) Data scaled with the initial drop radius  $R_0$  and viscous time  $t_v$ . Black solid line shows the best fit,  $R/R_0 = (1.84 \pm 0.13) \times (t/t_v)^{0.55 \pm 0.06}$ . Blue dashed line is for  $(0.57 \pm 0.05) \times \gamma/\eta$ . Black filled circles are the data of a silicone oil drop.

is also confirmed by finite element simulations in the Fig. 3, showing the final moments of the approach of a drop towards a liquid bath before coalescence. The gas is modelled using a lubrication equation, and incorporates the van der Waals driven disjoining pressure that causes the ‘jump to contact’. Fig. 3 shows that the bath is pushed down vertically  $\sim 100$  nm over the radial extent of the drop  $\sim \text{mm}$  before the drop ‘jumps to contact’, over a radial extent  $\sim 3 \mu\text{m}$  in  $\sim 0.1$  ms, similar to the mechanism seen in the drop-drop case but with a vertical shift. Unfortunately, resolving the nanometric scales associated with the jump-to-contact within Basilisk simulations is currently unachievable, so we attempt to mimic the predicted deformation by using the computed bath shape, vertically shift the sphere to account for the ‘jump’, and joining them with an artificial neck of 2.7  $\mu\text{m}$ ; further assuming that all liquid is initially motionless. This adjustment improves agreement between theory and experiment [Fig. 2, red dotted line], showing clearly that pre-contact dynamics can affect coalescence, even in cases where extreme care is taken to minimise the influence of the gas. However, a spatial shift remains necessary and appears to be due to our inability to resolve the very smallest scales, where there is a relaxation from pre- and post-contact dynamics over some length scale – providing clear motivation for future studies in this regime.

*Coalescence of colloidal-polymer liquid droplets.* Our system is a mixture of colloids and polymers dispersed together in the same liquid. Entropy-driven interactions create a phase separation between a colloid-rich and a colloid-poor (polymer-rich) phase, akin to a liquid-gas phase separation in a molecular system. For the latter, the order of magnitude of the surface tension is  $k_B T/d^2$ , with  $k_B$  the Boltzmann constant,  $T$  the temperature, and  $d$  the molecular size. For water, taking  $d = 2.5 \text{ \AA}$ , one finds a typical value for the surface tension of  $\approx 60 \text{ mNm}^{-1}$ , rather close to its actual value. For the colloidal system, the characteristic size is given by the colloid size; for  $d = 1 \mu\text{m}$ , one finds  $\gamma \approx 4 \text{ nNm}^{-1}$ , almost a million times smaller. According to the dimensional analysis above, this slows down the coalescence dynamics by a factor of one million and ‘slow’ video microscopy is sufficient to track the coalescence. The latter is done in a small flat capillary containing the colloidal liquid and gas phases, which are studied

by a confocal microscope tilted by 90 degrees, so that gravity maintains the phase separation.

By shaking the vessel, we obtain colloidal liquid droplets that slowly fall under the action of gravity allowing for coalescence with the bulk liquid [Fig. 4(a)]. Because in this mixture the coalescence is much slower, inertial effects only begin at a length scale of six meters. Hence, the coalescence is entirely dominated by viscosity. In agreement with this, we observe that for the first system ( $\gamma \approx 160$  nN/m), the liquid bridge grows linearly in time. This observation is consistent with the coalescence of simple fluids – namely, viscous silicone oil [Fig. 4(b)]. However, for the second system which has an ultra-ultralow surface tension ( $\gamma \approx 5$  nN/m), one of the most striking observations from the images is that in the formation of the liquid bridge, the roughness of the interface between the two phases is responsible for the initial merging of the drop with its bulk.

The coalescence is thus caused by the thermal fluctuations of the two surfaces, with multiple points of contacts between the two surfaces [Fig. 4(a), bottom panel] and  $R$  is measured from the total contact between the drop and the bulk from the different connected regions. This leads to a new fluctuation dominated regime in which the coalescence is much slower: the liquid bridge radius varies as  $R(t) \propto t^\beta$ , with  $\beta = 0.55 \pm 0.06$  from the best fit. This result is reminiscent of drop formation, the inverse process of coalescence where a drop detaches from another one. Also for such detachment, a fluctuation regime was uncovered, with an anomalous exponent that was significantly smaller than that for the viscous breakup regime [30].

Rather than such a linear time dependence, the fluctuation-driven breakup shows an increasing rate of pinching, just like here, and satisfies the predictions of a power law time dependence for fluctuation-driven pinch-off with a power close to the theoretical prediction of 0.42 [31], again similar to what is observed here. For the breakup the rationale for an exponent  $\beta$  smaller than unity with noise is when the bridge becomes smaller, the motion speeds up. As a result, random fluctuations are biased toward smaller bridge radii, consistent with a velocity  $t^{\beta-1}$ , which is singular. Similarly, during coalescence random fluctuations might fill the gap more quickly in



the early stages, and then slow down disproportionately.

In summary, there are two ways in which the initial contact between two drops can be established: interface fluctuations and jump-into-contact. The jump-into-contact is undetectable for the drop-drop experiment, likely because the air film can drain easily. However, it is very clearly present in the drop-on-bath experiment, where it generates capillary waves that determine the initial opening speed. Additionally, a combination of the two is also likely for macroscopic drops: thermal fluctuations can initiate disturbance of the interface, from which van der Waals forces can create a jump-into-contact. The former is observed in a system with ultralow interfacial tension and extremely small van der Waals forces, due to the vicinity of a critical point. Interestingly, similar observations have been made for the coalescence of water nanodroplets,

where fluctuations become more comparable to the drop size [32].

*Acknowledgements.* We are very grateful to the technology center of the university of Amsterdam for technical assistance with the electrical setup. DB thanks Jacco Snoeijer for very helpful discussions about the artifacts induced by side imaging. JES acknowledges the support of the EPSRC under grants EP/W031426/1, EP/S022848/1, EP/S029966/1, EP/P031684/1 and EP/V012002/1. Peter Lewin-Jones is supported by a studentship within the UK EPSRC-supported Centre for Doctoral Training in the Modeling of Heterogeneous Systems (HetSys), EP/S022848/1. For the purpose of open access, the author has applied a CC BY public copyright license to any Author Accepted Manuscript version arising from this submission.

- 
- [1] D. Lohse, Fundamental fluid dynamics challenges in inkjet printing, *Annual review of fluid mechanics* **54**, 349 (2022).
  - [2] A. Glasser, E. Cloutet, G. Hadzioannou, and H. Kellay, Tuning the rheology of conducting polymer inks for various deposition processes, *Chemistry of Materials* **31**, 6936 (2019).
  - [3] M. Liu, J. Wang, M. He, L. Wang, F. Li, L. Jiang, and Y. Song, Inkjet Printing Controllable Footprint Lines by Regulating the Dynamic Wettability of Coalescing Ink Droplets, *ACS Applied Materials & Interfaces* **6**, 13344 (2014).
  - [4] G. A. Somsen, C. van Rijn, S. Kooij, R. A. Bem, and D. Bonn, Small droplet aerosols in poorly ventilated spaces and sars-cov-2 transmission, *The Lancet Respiratory Medicine* **8**, 658 (2020).
  - [5] S. Kooij, C. van Rijn, N. Ribe, and D. Bonn, Self-charging of sprays, *Scientific Reports* **12**, 19296 (2022).
  - [6] R. Wanninkhof, W. E. Asher, D. T. Ho, C. Sweeney, and W. R. McGillis, Advances in quantifying air-sea gas exchange and environmental forcing, *Annual Review of Marine Science* **1**, 213 (2009).
  - [7] F. Raes, R. Van Dingenen, E. Vignati, J. Wilson, J.-P. Putaud, J. H. Seinfeld, and P. Adams, Formation and cycling of aerosols in the global troposphere, *Atmospheric environment* **34**, 4215 (2000).
  - [8] J. Eggers, J. R. Lister, and H. A. Stone, Coalescence of liquid drops, *Journal of Fluid Mechanics* **401**, 293 (1999).
  - [9] D. G. A. L. Aarts, H. N. W. Lekkerkerker, H. Guo, G. H. Wegdam, and D. Bonn, Hydrodynamics of Droplet Coalescence, *Physical Review Letters* **95**, 164503 (2005).
  - [10] J. D. Paulsen, J. C. Burton, and S. R. Nagel, Viscous to Inertial Crossover in Liquid Drop Coalescence, *Physical Review Letters* **106**, 10.1103/PhysRevLett.106.114501 (2011).
  - [11] M. Wu, T. Cubaud, and C.-M. Ho, Scaling law in liquid drop coalescence driven by surface tension, *Physics of Fluids* **16**, L51 (2004).
  - [12] S. T. Thoroddsen, K. Takehara, and T. G. Etoh, The coalescence speed of a pendent and a sessile drop, *Journal of Fluid Mechanics* **527**, 85 (2005).
  - [13] M. Wu, T. Cubaud, and C.-M. Ho, Scaling law in liquid drop coalescence driven by surface tension, *Physics of Fluids* **16**, L51 (2004).
  - [14] A. Eddi, K. Winkels, and J. Snoeijer, Influence of droplet geometry on the coalescence of low viscosity drops, *Physical review letters* **111**, 144502 (2013).
  - [15] J. D. Paulsen, Approach and coalescence of liquid drops in air, *Physical Review E* **88**, 063010 (2013).
  - [16] J. E. Sprittles and Y. D. Shikhmurzaev, A parametric study of the coalescence of liquid drops in a viscous gas, *Journal of Fluid Mechanics* **753**, 279 (2014).
  - [17] C. R. Anthony, M. T. Harris, and O. A. Basaran, Initial regime of drop coalescence, *Physical Review Fluids* **5**, 033608 (2020).
  - [18] S. C. Case, Coalescence of low-viscosity fluids in air, *Phys. Rev. E* **79**, 026307 (2009).
  - [19] J. D. Paulsen, J. C. Burton, S. R. Nagel, S. Appathurai, M. T. Harris, and O. A. Basaran, The inexorable resistance of inertia determines the initial regime of drop coalescence, *Proceedings of the National Academy of Sciences* **109**, 6857 (2012).
  - [20] <http://basilisk.fr/>, .
  - [21] S. Popinet, Quadtree-adaptive tsunami modelling, *Ocean Dynamics* **61**, 1261 (2011).
  - [22] J. E. Sprittles, Gas microfilms in droplet dynamics: When do drops bounce?, *Annual Review of Fluid Mechanics* **56** (2024).
  - [23] R. Ledesma-Alonso, P. Tordjeman, and D. Legendre, Multiscale deformation of a liquid surface in interaction with a nanoprobe, *Phys. Rev. E* **85**, 061602 (2012).
  - [24] R. Ledesma-Alonso, D. Legendre, and P. Tordjeman, Nanoscale deformation of a liquid surface, *Phys. Rev. Lett.* **108**, 106104 (2012).
  - [25] V. Chireux, M. Protat, F. Risso, T. Ondarçuhu, and P. Tordjeman, Jump-to-contact instability: The nanoscale mechanism of droplet coalescence in air, *Phys. Rev. Fluids* **3**, 102001 (2018).
  - [26] V. Chireux, P. Tordjeman, and F. Risso, Bridge expansion after coalescence of two droplets in air: Inertial regime, *Physics of Fluids* **33**, 062112 (2021).
  - [27] K. G. Winkels, J. H. Weijs, A. Eddi, and J. H. Snoeijer, Initial spreading of low-viscosity drops on partially wetting surfaces, *Phys. Rev. E* **85**, 055301 (2012).
  - [28] L. Duchemin, J. Eggers, and C. Josserand, Inviscid coalescence of drops, *Journal of Fluid Mechanics* **487**, 167 (2003).
  - [29] D. G. A. L. Aarts, M. Schmidt, and H. N. W. Lekkerkerker, Direct visual observation of thermal capillary waves, *Science* **304**, 847 (2004), <https://www.science.org/doi/pdf/10.1126/science.1097116>.
  - [30] Y. Hennequin, D. G. A. L. Aarts, J. H. van der Wiel, G. Wegdam, J. Eggers, H. N. W. Lekkerkerker, and D. Bonn, Drop formation by thermal fluctuations at an ultralow surface tension, *Phys. Rev. Lett.* **97**, 244502 (2006).
  - [31] J. Eggers, Dynamics of liquid nanojets, *Phys. Rev. Lett.* **89**,

084502 (2002).

- [32] S. Perumanath, M. K. Borg, M. V. Chubynsky, J. E. Sprittles, and J. M. Reese, Droplet coalescence is initiated by thermal motion, *Physical review letters* **122**, 104501 (2019).

## SUPPLEMENTARY MATERIALS

### I. DROP-DROP

#### A. Basilisk Simulations.

Work has been carried out on dimensionless variables using the drop radius, surface tension and density of the liquid as the basis for non-dimensionalizing. In the numerical study, gravitational forces were neglected. Axisymmetric simulations are performed in a cylindrical coordinate system  $(\bar{r}, \bar{z})$  in a box of length  $L$  where the axis of symmetry lies along the  $z$ -axis (the left boundary of the box).

In the 2 drops case, the symmetry of the problem has been exploited to reduce the computational cost. A numerical domain of length  $L=1.1$  was chosen in which one of the drops centered at the point  $(0, -0.1)$  was placed [see figure 5 (a)]. A symmetry condition was imposed on the bottom boundary to model the other drop. The two drops were brought into contact by an artificial neck with a radius of 0.0028. Initially, both fluids (liquid and gas) are at rest. The cells in Basilisk are square, so an initial mesh with a maximum refinement of 18 was used in the contact zone to model the collapse of the droplets in the early stages. As the meniscus formed and retracted, this maximum refinement level was reduced.

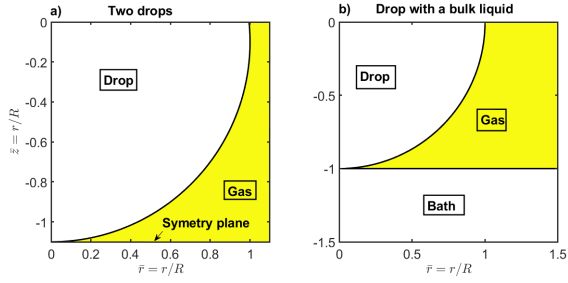


FIG. 5. **Numerical domains.** (a) Shows the numerical domain for the two drops case while (b) shows the numerical domain used for the drop-bath case.

#### Numerical computation of the electrical resistance

The numerical resistance was computed using a combination of Basilisk simulations and a finite element method. The methodology used is briefly described below.

First, at the selected time at which the resistance is computed, the numerical profile of the interface is extracted from the Basilisk simulation and saved into a text file. This file is then imported to MATLAB to generate the closed domain needed to solve the Laplace equation for electrical problem. The geometry is normalized with  $R_{min}$ , and centered at the axial position where the interface has its minimum radius. Neumann boundary conditions are applied on the free surface and on the axis while Dirichlet boundary conditions are applied on the solid supports. A normalized drop in the electrical potential equal to one was considered. Then, the Laplace equa-

tion is discretized and solved using a finite element method provided by MATLAB PDE tool. Once we got the electrical potential, the constant and normalized current flow (intensity) through the system is obtained by integrating the axial derivative of electrical potential at any axial position, assuming an electrical conductivity equal to one. Finally, the numerical electrical resistance is simply computed by dividing the intensity by  $R_{min}$ . See [1] for further details of the procedure.

#### B. Finite element simulations

Whilst Basilisk is able to accurately capture the post-merging coalescence event, volume of fluid techniques are not well suited to resolving the pre-contact ‘collision’ phase to determine the initial contact dynamics. Here, we use the finite element approach described in detail in [22], focusing it on low-speed collisions as opposed to its usual application to higher speed impacts.

The computational model is based on solving the Navier-Stokes equations in the bulk of the drop/bath coupled to a lubrication description of the gas phase. Due to the small film heights encountered, gas kinetic effects are accounted for, and are often crucial, alongside van der Waals forces between the two distinct volumes (drop-drop or drop-bath) that will act to pull the interfaces together. The governing equations are then solved using an open-source finite element package oomph-lib [3] based on the arbitrary Lagrangian Eulerian approach which, crucially, permits a high accuracy representation of the free surface and is well suited to multiscale problems like this one. Complete details are provided in [22].

Here, we take the experimental values, using material parameters for the water-air system alongside a collision speed of  $5 \times 10^{-6}$  m/s and, due to its negligible effect on the ‘jump to contact’, neglect gravity. In Fig. 6 the profiles of the interface shape as the two drops approach one another show that there is very little deformation due to the gas but that the van der Waals forces between the two interfaces causes a ‘jump to contact’ when their separation is  $\approx 30$ nm which deformed the drop on a lateral scale of  $\sim \mu\text{m}$ ’s.

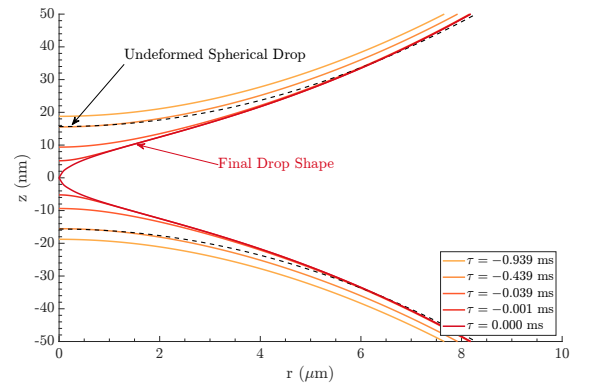


FIG. 6. Computed interface profiles of a drop-drop case as the drops approach and then make first contact at  $\tau = 0$ .

### C. Electrical setup

We measured the resistance of the opening of the neck neck with an electrical circuit analogous to the one described in the references ([10, 18, 19]).

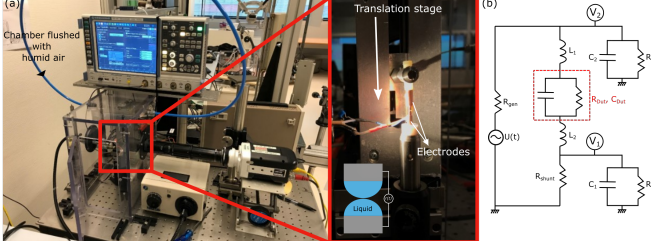


FIG. 7. **Electrical setup used for the measure of the electrical resistance of the coalescence event.** (a) The entire setup is placed in a chamber flushed continuously with humid air to prevent evaporation. A close view of the two electrodes receiving the two droplets. The upper electrode can be translated downward thanks to a speed-controlled translation stage. The dynamics of coalescence is followed, over a large time scale, by measuring the electrical resistance (oscilloscope on the top) and by imaging (fast camera) the capillary bridge. (b) Equivalent electrical circuit.

The voltages  $V_1$  and  $V_2$  were measured and sampled simultaneously at a rate of 1 GHz. The frequency  $f$  of the input sine wave from the function generator is taken at a maximum value of  $f = 10$  MHz, allowing to reach sub-microsecond time scales. Higher frequencies result in the voltages were read in Matlab and analyzed with a homemade routine. The analysis averaged the incoming signals over a single period to find the ratio of their amplitudes,  $V_2/V_1$ , as a function of time  $t$ . In addition, the analysis compared the input signals to a known sine wave and found the relative phase shift of each signal versus time. We chose a maximum amplitude of voltage of 1 V to prevent the deformation of the droplet's interfaces when brought into contact (see Sup. Fig. 9).

#### 1. Relation between the electrical resistance and the neck diameter

The minimum neck diameter  $R$  is obtained indirectly by measuring the electrical resistance  $r$  of the neck in time. To obtain the minimum neck diameter, we use the equation 1 proposed by [10]:

$$R = 2 \left[ \left( r - \frac{1}{\pi R_0 \sigma} \right) 3.62 \sigma \right]^{-1} \quad (1)$$

We confirmed the validity of this equation with our simulations by plotting the electrical resistance obtained from our Basilisk simulation as a function of the minimum neck diameter. The results presented in Figure 8 confirmed the good agreement between the two. We thus use this equation to convert the measured electrical resistance from our experiments to the physical minimum neck diameter  $R$ .

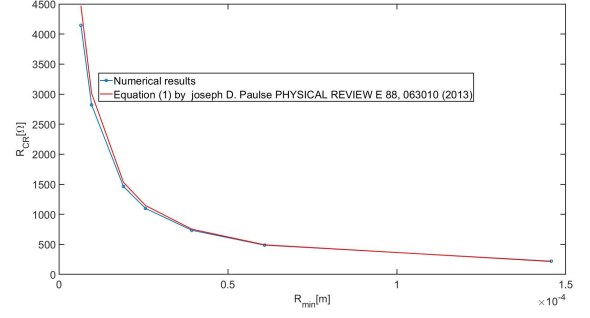


FIG. 8. **Relation between electrical resistance and the minimum neck diameter.** The red solid line are results obtained from the Eq. 1 and the blue solid line is obtained from our Basilisk simulations.

#### 2. Effect of charges and high voltage on the drops' interface and coalescence dynamics.

Fig. 9 compares charged and non-charged water drops as they approach each other. Initially, two water drops with similar sizes formed on the tips of two vertical plastic nozzles (diameter 2.3 mm). Similar to the setup used in the electric measurement, we fixed the bottom drop while moving the top drop towards the bottom one. Fast imaging was applied from the side using an optical zoom lens ( $20 \times$  magnification). To charge the drops, we simply used a charged plastic tube (through rubbing with dry hair) to get close to the drops before coalescence occurred.

When the drops are charged, a sharp liquid neck appears in the early moments of coalescence (Fig. 9b). This charge effect causes a deviation in dynamics from the non-charged case, which follows the capillary-inertial scaling,  $R(t) \sim t^{1/2}$  (Fig. 9a). Instead, in the early stages, the liquid neck linearly grows for the charged drops. This pointed shape could also occur in drop-drop electric measurements where an external electric field is applied, potentially explaining the observation of a linear regime in the work of Paulsen *et al.* [10]. However, in our drop-drop electric measurement, before triggering coalescence, we carefully used a zero-static gun to discharge the drops, ruling out the pointed shapes.



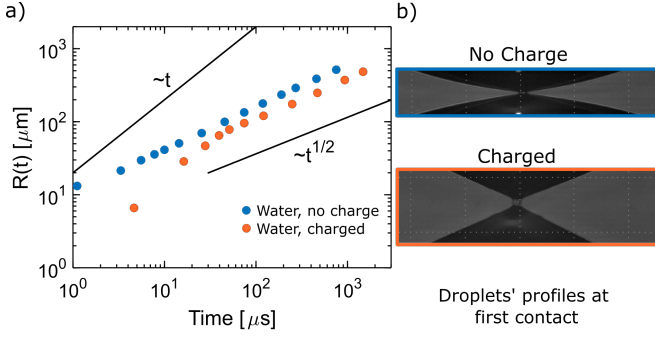


FIG. 9. **Effect of surface charges on the dynamics of coalescence of water droplets (imaging).** (a) The presence of charges on water droplets (orange symbols) is shown to influence the coalescence dynamics at early stages, compared to the uncharged case (blue symbols). Note that, the initial drop sizes in these two experiments are slightly different. (b) Snapshots of the profiles at the first contact of coalescence, highlighting the difference between the two cases.

## II. DROP-BULK

### A. Basilisk Simulations

In this case, a computational domain of length  $L=1.5$  has been chosen in which the droplet is centred at point  $(0,0)$ . A liquid bath with a free and flat surface was added at a height  $\hat{z} = z/R = -1$ . The drop and the bath were brought into contact by an artificial neck with a radius of 0.003. An initial mesh with a maximum refinement of 19 was used in the contact zone to model the collapse of the droplet with the bath in the early stage. Again, as the meniscus formed and retracted, this maximum refinement level was reduced.

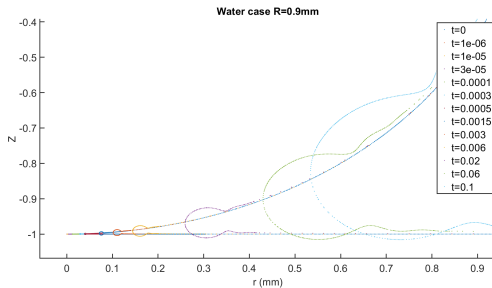


FIG. 10. Simulated (Basilisk) interface profiles for different times after coalescence in the drop-bulk configuration. Note the formation and the growth of the air pocket followed by waves.

An additional simulation (labeled ‘deformed’ in Fig. 2d) instead used the bath profile computed at the moment of contact by the finite element simulation in Fig. 3, where the bath has been forced down  $\sim 100$  nm. The spherical drop was also shifted vertically down so that at  $r = 0$  the vertical distance between the drop and the bath is the same as that found by the finite element simulation before the ‘jump to contact’ occurred ( $t = -0.08$  ms in Fig. 2) An artificial neck of radius 0.003 was then added (the same as the ‘undeformed’ case).

### B. Finite element simulations

Fig. 2 for the drop-bath case in the main text shows that the drop exhibits a rather similar shape to those recovered for the drop-drop case, with a notable ‘jump to contact’. However, the deformation of the bath is more prominent, with a ‘dip’ of  $\sim 100$  nm below its initial height seen when contact occurs. This is because Laplace pressure associated with the planar, or slightly deformed, bath interface is significantly lower than the drop’s and therefore the gas lubrication pressure has more of an influence on it – one can see from the figure that this deformation has occurred well before the final stages of contact and the inset shows that it extends radially to the width of the drop,

### C. Imaging setup

As mentioned in the main text, to access the initial stages of coalescence optically, we deploy a novel approach by viewing the event from ‘underneath’ to overcome spurious effects due to the side imaging [14, 27]. The setup consists of a drop on a needle to which liquid is supplied slowly by a syringe pump (Harvard Apparatus). This drop is facing a bath of the same liquid (See Fig. 11). Our needle tip is typically millimetric (diameter 1.37 mm) and a drop is slowly grown at its tip until it coalesces with the bulk (growing velocity  $\leq 20 \mu\text{m/s}$ , in an attempt to minimize the effect of air drainage between the droplet and the bulk surface). To change the properties of the fluids, different amounts of glycerol were mixed with deionized water (Milli-Q). The viscosity, density and surface tension are given in the Supplementary Table S1. All experiments were performed at room temperature ( $22 \pm 1$  °C) and atmospheric pressure.

The growth of the neck bridging the droplet with its bulk is recorded from below through the bath using an inverted microscope (Zeiss Axiovert A1) at a frame rate of up to 1,000,000 frames per second (fps) using a high-speed camera (Phantom TMX 7510) allowing us to reach a spatial resolution of typically  $0.9 \mu\text{m/pix}$  with a  $20\times$  microscope objective (Zeiss long working distance WD = 20mm).

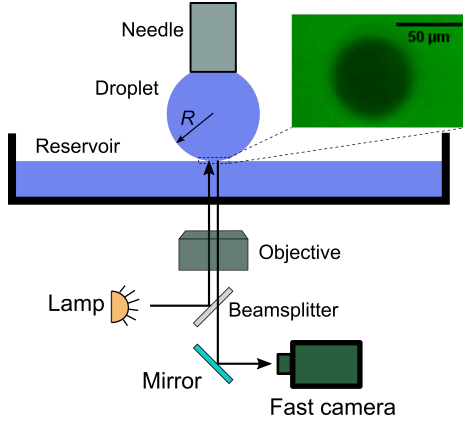


FIG. 11. **Experimental setup for drop-bulk coalescence.** The setup combined a microscope (Zeiss Observer) coupled to a fast camera with different magnifications.

Before coalescence, we observe interference fringes between the two surfaces in the last instances before coalescence (see Sup. Fig. 12), which suggest the presence of a thin air film which acts as a lubricant between the two approaching surfaces. This air film continually thins, and if it becomes thin enough, the two surfaces jump into contact.

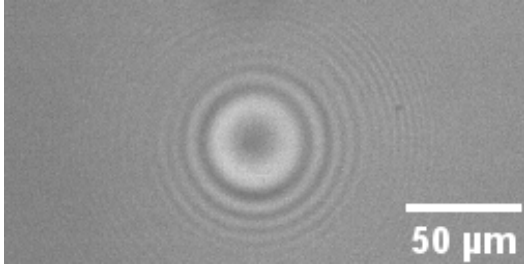


FIG. 12. **Fringes at the drop-bath interface before the drop coalesces with the bulk.**

Table I shows the properties of fluids used in this study. Different glycerol fractions (by mass) were mixed with deionized water to tune the viscosity. The density and surface tension of the mixture were estimated according to the reference [2].

Fluids	Glycerol fraction $\phi$ [wt%]	Viscosity $\eta$ [mPa·s]	Surf. Tension $\gamma$ [mN/m]	Density $\rho$ [g/mL]	Conductivity $\sigma$ [S/m]
Water + NaCl	0	1.78	82	1.12	30
Water	0	1	72	1	-
Water+Glycerol	25	2.16	71	1.06	-
Water+Glycerol	50	5.71	69	1.13	-
Water+Glycerol	60	11.5	68	1.15	-

TABLE I. Liquid properties used in the electrical (drop-drop) and imaging (drop-bulk) experiments.

- 
- [1] A. Deblais, et al., Viscous effects on inertial drop formation, Physical review letters **121**, 254501 (2018).
  - [2] T. Koichi, et al., Physical properties of aqueous glycerol solutions, Journal of Petroleum Science and Engineering **98**, 50–60 (2012).
  - [3] M. Heil, et al., Oomph-Lib, <https://github.com/oomph-lib/oomph-lib> **98**, (2022).